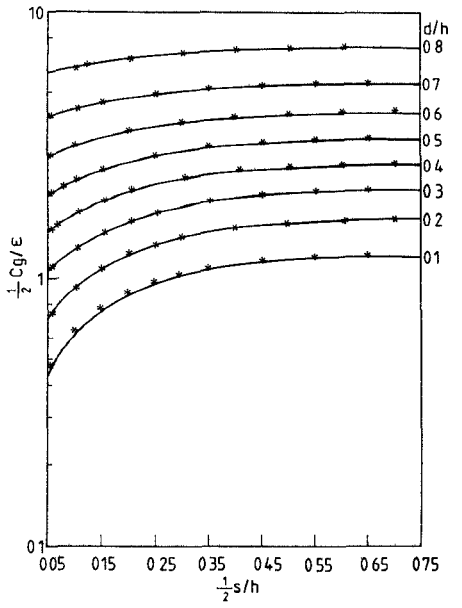

Fig. 5. Comparison between $C_g/(2\epsilon)$ as computed in [3] (continuous line) and the computed values here obtained (stars).

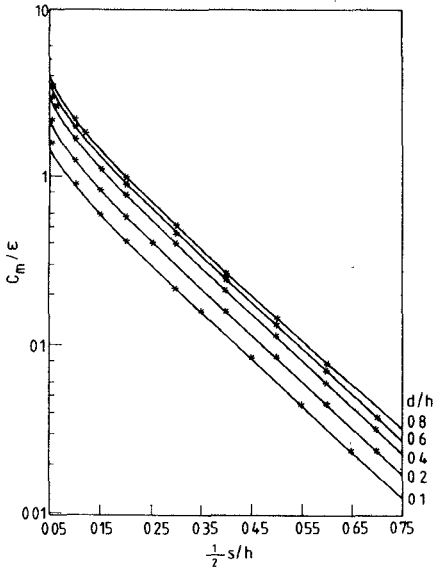

Fig. 6. Comparison between C_m/ϵ as computed in [3] (continuous line) and the computed values here obtained (stars).

Notice that the above expressions give a satisfactory approximation of the actual admittances (maximum percent error less than 1 percent [3]) only for $d/h < 0.3$ and $s/d > 2$, which are quite below the limits on d/h and s/d considered in the interpolating formulas given in this paper.

C. Comparison with the Numerical Results Given in [3]

Figs 2 and 3 in [3] show the numerical results obtained by Cristal for the structures in Fig. 3(a) and (b), as static capacitances C_g/ϵ and C_m/ϵ, where $C_m = 1/2C_s$.

For the purpose of comparison, the numerical results obtained here have been transformed into the same form given by Cristal. With the same procedure adopted in Section V-B, we obtain from (11) and (12)

$$Y'_{co} = 2Y_{co} - Y_c \tag{15}$$

$$Y'_{ce} = 2Y_{ce} - Y_c. \tag{16}$$

As a consequence, the Cristal's parameters C_g/ϵ and C_m/ϵ may be written as a function of Y_{co}, Y_{ce}, and Y_c

$$C_g/\epsilon = Z_\infty(2Y_{ce} - Y_c) \tag{17}$$

$$C_m/\epsilon = Z_\infty(Y_{co} - Y_{ce})/2. \tag{18}$$

The graphs of [3] for $\frac{1}{2}C_g/\epsilon$ and C_m/ϵ are shown in Figs. 5 and 6 together with some points representing the numerical results obtained in this work, transformed for the structure of Fig. 3 by means of (17) and (18). The figures show a very good agreement between the results obtained with the numerical method followed in this paper and those given by Cristal.

VI. Conclusion

A numerical evaluation of the characteristic impedance of slab line and of two derived transmission lines has been presented. The results obtained in the case of these two structures also represent the even and odd characteristic impedance of two coupled slab lines.

The results obtained show a very good agreement when compared with the few available data in the literature. An extensive comparison of the computed values has been made, in particular with the data presented by Chisholm [2] and Cristal [3]. In addition, the overall accuracy of the numerical method employed has been estimated and seems better than 1 percent for the computed values of the characteristic impedance of all the transmission lines considered, when $d/h \leqslant 0.9$ and $s/d \geqslant 0.1$.

Closed-form expressions for the characteristic impedances considered here have also been presented, and were obtained by interpolating the numerical values. The precision of these expressions, if compared with the numerical values, is better than 1 percent for the characteristic impedance of the slab line and about 1.5 and 3 percent for even and odd characteristic impedance of coupled slab lines, respectively.

References

[1] G. B. Stracca, G. Macchiarella, G. Dolci, and M. Politi, "Design formulas for coupled slab lines," *Alta Frequenza*, vol. 54, pp. 346–352, Dec. 1985.
[2] R. M. Chisholm, "The characteristic impedance of trough and slab lines," *IRE Trans. Microwave Theory Tech.*, vol. MTT-4, pp. 166–177, July 1956.
[3] E. G. Cristal, "Coupled circular cylindrical rods between parallel ground planes," *IRE Trans. Microwave Theory Tech.*, vol. MTT-12, pp. 428–439, July 1964.
[4] S. Frankel, "Characteristic impedance of parallel wires in rectangular troughs," *Proc. IRE*, vol. 30, pp. 182–190, Apr. 1942.
[5] J. T. Bolljahn and G. L Matthaei, "A study of the phase and filter properties of arrays of parallel conductors between ground planes," *Proc. IRE*, vol. 50, pp. 299–311, Mar. 1962.
[6] R. Levy, "Directional couplers," in *Advances in Microwaves*, vol. 1. New York: Academic Press, 1966, pp. 115–209.

Shunt-Connected Microstrip Radial Stubs

F. GIANNINI, SENIOR MEMBER, IEEE, M. RUGGIERI, AND J. VRBA

Abstract **— Radial-line stubs provide an interesting alternative to low-impedance conventional straight stubs. They are useful as filter elements in both series and shunt configurations. In this short paper, the planar circuit**

Manuscript received July 8, 1985; revised October 25, 1985.

F. Giannini and M. Ruggieri are with the Dipartimento di Ingegneria Elettronica, II Universita Degli Studi di Roma, Via Orazio Raimondo 00173, Roma, Italy.
J. Vrba is with the Department of Electromagnetic Field, Czech Technical University, 16627 Praha, Czechoslovakia.

IEEE Log Number 8406855.

analysis previously performed for a series-connected radial stub is extended to the shunt configuration. Theoretical and experimental results are presented to verify the equivalent model for the shunt-connected radial stub.

Radial stubs are widely used in many microstrip circuits, such as matching networks, bias lines, low-pass filters, etc., where both an accurate localization of a zero-point impedance and a very low level of characteristic impedance is needed.

The formula proposed by Vinding [1] provides reasonable results at lower frequencies and for radial stubs on low dielectric substrates [2], [3]. However, for high-dielectric constant materials, such as alumina or GaAs, substantial discrepancies appear, and the simple formula [1], which involves actual dimensions and dielectric constants, cannot be used any longer. Such a problem can be dealt with introducing the effective geometries and by using the so-called dynamic permittivities [4], as it has been demonstrated for similar structures. In an earlier paper [5], a planar circuit analysis of a microstrip radial stub has been presented. The method, based on the electromagnetic (EM) field expansion in terms of resonant modes of radial structure, gives an effective characterization of the radial-line stubs for design purposes. In particular, the definition of an equivalent characteristic impedance has shown the suitability of such a structure as an alternative of low-impedance straight stub.

In this short paper, the method of analysis previously performed for a series-connected radial stub [5] is extended to the shunt connection.

In the cases of shunt and series connections, in fact, the effects of the fringing fields related to the electromagnetic structures are significantly different. Consequently, radial stubs with the same actual geometries result in equivalent structures with different effective geometries, depending on the kind of configuration.

According to the electromagnetic field expansion in terms of resonant modes, and assuming that only TM modes, i.e., modes with only a radial dependance, are excited [5], the input impedance of a lossless microstrip radial stub can be expressed as

$$Z_{in} = -j\frac{k_g P_{00}^2}{k^2 \epsilon_{d,0}} + jk_g \sum_{n=1}^{\infty} \frac{P_{0n}^2}{k_{0n}^2 - k^2 \epsilon_{d,n}} \tag{1}$$

where k_g is the wavenumber corresponding to a microstrip line of width W_g, $k = \omega\sqrt{\mu\epsilon}$ is the free-space wavenumber, and $\epsilon_{d,n}$ and k_{0n} are the dynamic effective permittivity and the eigenvalue of the TM_{0n} modes. P_{0n} are the coupling coefficients between the transmission line and the TM_{0n} resonant modes and are given by [5][1]

$$P_{0n} = \sqrt{W_{ge}}\left[A_{0n} J_0(k_{0n} r_{ie}) + B_{0n} N_0(k_{0n} r_{ie})\right] \tag{2}$$

$$P_{00} = \sqrt{\frac{2W_{ge}}{\alpha(r_{0e}^2 - r_{ie}^2)}} \tag{3}$$

where

$$A_{0n} = \sqrt{\frac{2}{\alpha}}\left\{ r_{0e}^2\left[J_0(k_{0n} r_{0e}) + K_n N_0(k_{0n} r_{0e})\right] - r_{ie}^2\left[J_0(k_{0n} r_{ie}) + K_n N_0(k_{0n} r_{ie})\right]^2\right\}^{-1/2} \tag{4}$$

$$B_{0n} = K_n A_{0n} \quad K_n = -\frac{J_1(k_{0n} r_{0e})}{N_1(k_{0n} r_{0e})} \tag{5}$$

where J_0, J_1, N_0, and N_1 are the Bessel and Neumann functions of the order 0 or 1.

[1]Note that some minor printing errors in [5, eqs (4) and (5)] are here corrected

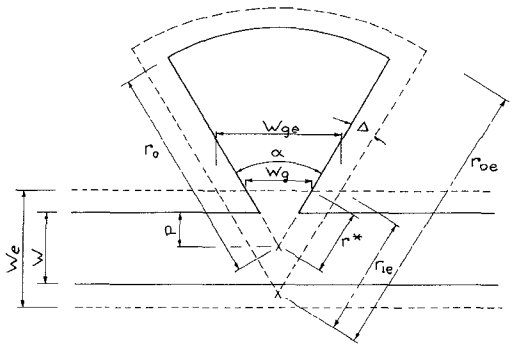

Fig. 1. Geometries of a shunt-connected microstrip radial stub.

In Fig. 1, both the actual and effective geometries of a shunt-connected radial stub are shown. It is worth noting in particular that, unlike a series-connected radial stub for which the width of the input port is independent of α, the width W_g of the shunt-connected radial stub input port can greatly increase with angle α, principally due to the effective width W_e of the transmission line. In this case, it can no longer be assumed that the incoming EM field is uniform on the whole port. Also, modes other than TM_{0n} can exist on the radial stub and, therefore, a more complicated field expansion has to be used to explain the frequency behavior of the radial structure

Assuming the angle α subtended by the stub is less than 90° and with a proper choice of dimension P, i.e., the depth of the insertion of the circular sector in the transmission line, the simplified theory presented here can be used to achieve very accurate results.

Referring to Fig. 1, the actual geometry of the transmission line with a shunt-connected radial stub can be described in terms of the width W of the transmission line, depth P of the insertion of the circular sector with angle α, and outer radius r_o.

Fromthese parameters, effective dimensions are easily obtained as follows:

$$r^* = \frac{2P + W_e - W}{2\cos\frac{\alpha}{2}}, \qquad W_e = f(W) \tag{6}$$

$$\Delta = \frac{f(\alpha r^*) - \alpha r^*}{2} \tag{7}$$

$$W_g = (2P + W_e - W)\cdot\tan\frac{\alpha}{2} \tag{8}$$

$$W_{ge} = W_g + \frac{2\Delta}{\cos\frac{\alpha}{2}} \tag{9}$$

$$r_{ie} = r^* + \frac{2\Delta}{\sin\alpha} \tag{10}$$

$$r_{0e} = r_0\left[1 + \frac{2h}{\pi r_0}\ln\left(\frac{\pi r_0}{2h}\right) + 1.7726\right]^{1/2} + \frac{\Delta}{\sin\frac{\alpha}{2}} \tag{11}$$

where $f(W)$ and $f(\alpha r^*)$ are the effective width of two microstrip lines of actual width W and αr^*, respectively.

This model has been tested on several microstrip structures with two identical radial stubs shunt-connected to the transmission line (the so-called "butterfly" stub) with outer radii $r_o = 0.3$, 0.5, and 0.75 cm, depth of insertion $P = 0.01$ and 0.03 cm, and central angle $\alpha = 30°$, 60°, 90°, and 120°. All the above-men-

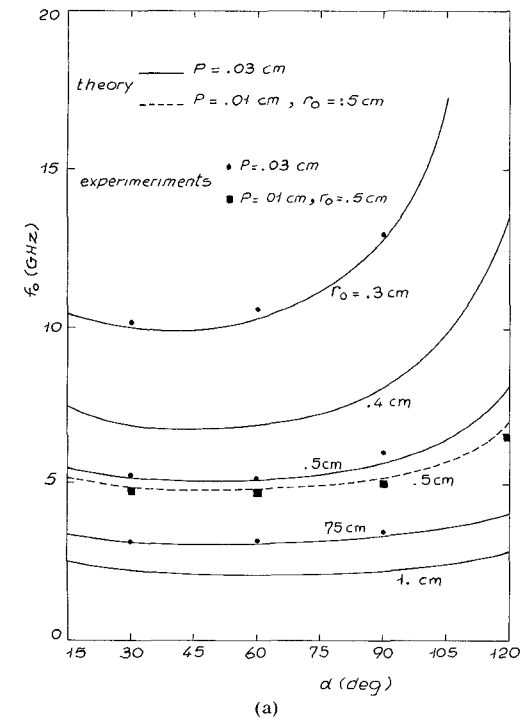

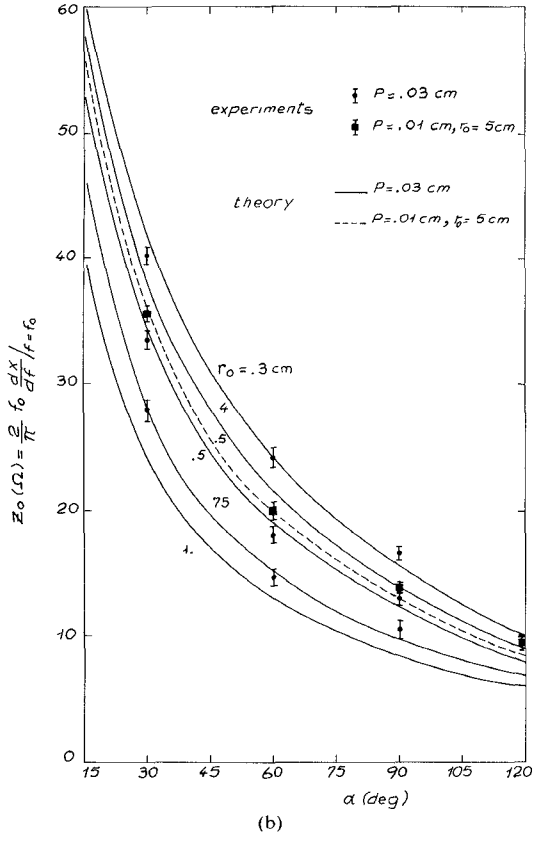

Fig. 2. (a) Frequency of the zero input impedance and (b) equivalent characteristic impedance versus sector angle α for a shunt-connected radial stub All the experiments have been performed on a 0.0635-cm-thick alumina substrate ($\epsilon_r = 10$).

tioned stubs have been realized on 0.0635-cm-thick alumina substrate having $\epsilon_r = 10$.

Fig. 2(a) shows the calculated and measured frequency f_0, at which the first zero of input reactance X of a shunt-connected radial stub occurs. The calculations take into account five TM_{0n} radial modes. The measurements are performed on a HP 8510A vector network analyzer.

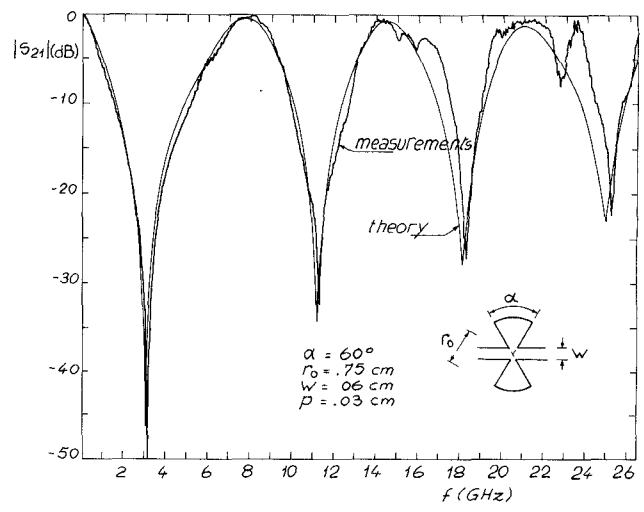

Fig. 3 Frequency behavior of scattering parameter $|S_{21}|$ for a "butterfly" stub. $\alpha = 60°$, $r_0 = 0.75$ cm, $P = 0$ 03 cm

Fig. 2(b) shows the dependance of the equivalent characteristic impedance Z_0 of the radial stub as a function of α. Z_0 is given by the relation [5]

$$Z_0 = \frac{2f_0}{\pi} \cdot \frac{dX}{df}\bigg|_{f=f_0}. \tag{12}$$

As can be seen, a good agreement has been obtained between theory and experiments, in particular, for lower values of α and depth of insertion P. The EM fields on the input port of the radial stubs under these conditions can be assumed to be uniform and, hence, the TM_{0n} modes are only excited.

If the input port of the radial stub increases either with an increase in the angle α or with the depth of the insertion P, transverse modes TM_{mn} may be excited causing a shift in its frequency response.

Moreover, it is worth noting the significant influence of the depth of insertion P. In the case of a 50-Ω transmission line, the change of the parameter P from 300 to 100 μm results in variations of f_0 from about 10 to 20 percent when α is varied from 15° to 120°.

Finally, in Fig. 3, the calculated and measured frequency behavior of $|S_{21}|$ of a "butterfly" stub ($r_0 = 0.75$ cm, $P = 0.03$ cm, and $\alpha = 60°$) in the frequency band 45 MHz–26.5 GHz is shown. Theoretical and experimental calculations and measurements take into account only the losses of the radial stub, while those of the transmission line have been eliminated through the measurement setup. It also follows that for frequencies approximately up to 14 GHz, the assumed excitations of only the TM_{0n} modes is correct, and the agreement between measurements and calculations is good. However, at higher frequencies, the effect of TM_{mn} modes (other then TM_{0n} modes) is not negligible, even if the nature of both curves are similar. The theoretical results of Fig. 3 are preliminary ones and represent a further development of the present method that is being extended to the case of a lossy structure.

The method of planar network analysis previously presented for a series-connected radial stub has been extended to the shunt configuration.

In particular, it was pointed out that due to the different effects of the fringing fields, the equivalent model corresponding to a shunt-connected stub is quite different from the one corre-

sponding to a series-connected radial stub with the same actual dimensions, thereby giving significant differences in the frequency behavior of the two structures.

Finally, the effectiveness of the method is stressed by the presentation of preliminary theoretical results obtained by an extension of the planar approach to the case of a lossy radial stub.

References

[1] J. P. Vinding, "Radial line stubs as elements in strip line circuits," in *NEREM Rec.*, 1967, pp. 108–109

[2] H. A. Atwater, "Microstrip reactive circuit elements," *IEEE Trans. Microwave Theory Tech.*, vol. MTT-31, pp. 488–491, June 1983.

[3] A. Chu *et al.*, "GaAs monolithic frequency doublers with series connected varactor diodes," in *1984 IEEE MTT-S Int. Microwave Symp. Dig.*, pp. 51–54.

[4] J. Vrba, "Dynamic permittivities of microstrip ring resonators," *Electron. Lett.*, vol. 15, no. 16, pp. 504–505, Aug. 1979.

[5] F. Giannini, R. Sorrentino, and J. Vrba, "Planar circuit analysis of microstrip radial stub," *IEEE Trans. Microwave Theory Tech.*, vol. MTT-32, pp. 1652–1655, Dec. 1984.

The Effects of Attenuation on the Born Reconstruction Procedure for Microwave Diffraction Tomography

FRANK J. PAOLONI, MEMBER IEEE

Abstract—**The effects of attenuation on the Born inversion process for diffraction tomography are investigated. The exact forward scattered fields for a lossy dielectric cylinder in a lossy medium are calculated and are then used to reconstruct an image of the scattering object. An accurate image is produced only when the cylinder acts as a small perturbation on the dielectric constant of the external medium. Results indicate that even small losses have a significant effect on the resolution of the image. It is possible, however, to eliminate image distortion by matching the loss tangent of the outside medium to that within the cylinder.**

I. Introduction

Diffraction tomography provides a method of reconstructing the cross section of dielectric objects that may be useful for medical imaging of soft tissues or other applications [1]–[3]. The forward scattered fields of the object are measured for a variety of angles of incidence of a plane wave, and an inversion procedure is used to recreate the scattering centers within the object. The inversion uses approximations that are strictly valid only when the object is weakly scattering and there are no loss mechanisms. Recently, Slaney, Kak, and Larson [3] have made a computational study of the limitations of inversion processes based on the Born [4]–[6] and Rytov [7] approximations by using the exact scattered fields of a perfect uniform dielectric cylinder. They found that the accuracy of the reconstructed image is strongly determined by the dielectric constant of the cylinder relative to the uniform medium outside (ϵ_r) and by its diameter relative to the wavelength of the incident electromagnetic wave. The calculations, however, assume that there are no losses within the dielectrics although it is recognized that in the practical situation severe attenuation can occur.

In this paper, we study the effects of object and medium attenuation on diffraction tomographic reconstruction based on the Born approximation. Conditions under which distortions of the image are minimized are also investigated.

Manuscript received July 16, 1985; revised October 28, 1985. This work was supported in part by the Australian Research Grant Scheme, Australian Telecommunications and Electronics Research Board, and University Research Grant Committee.

The author is with the Department of Electrical and Computer Engineering, University of Wollongong, Wollongong, NSW 2500, Australia

IEEE Log Number 8406351.

II. Brief Outline of the Numerical Procedure

The Born approximation [1–6] assumes that the incident fields within the object are the same as when the object is absent and the object is considered to be a tenuous collection of point scatterers. Using the Greens function for spherical waves in a uniform lossless medium, a closed-form relation in the Fourier plane can be derived between the external forward scattered field and the dielectric constant distribution within the object. One way to study the effects of attenuation on this relationship is to choose a particular geometry where the exact scattered fields can be calculated when losses are included both within the object and in the uniform medium outside. Reconstruction of the distribution of scatterer using the Born approximation will then reveal the resolving power of the process.

The formulation of the boundary-value problem for a plane wave incident on a lossy dielectric cylinder with the electric field parallel to the axis of the cylinder is identical to the lossless case [8], with the exception that the external scattered fields are an infinite sum of Hankel functions of complex arguement. The major computational difficulty is to accurately evaluate these functions of large order and large complex argument.

The scattering centers within the cylinder can be derived from the external diffraction fields using the Born approximation in a manner similar to that of Slaney *et al.* [3]. The program steps are as follows.

1) Take the Fourier Transform of the scattered fields

$$E(S_x) = F[E(x)].$$

2) Multiply by the back propagation filter $f(S_x)$ [9]

$$f(S_x) = -2jk_0 m \exp(-jk_0 mR) \tag{1}$$

where

$$m = \sqrt{1-(\lambda_o S_x)^2},$$

R = perpendicular range of field measurements behind cylinder axis,

$k_0 = 2\pi/\lambda_0$ = wavenumber in medium outside cylinder.

3) Deposit the result onto the two-dimensional (S_x, S_z) Fourier space of the object function along a semicircle of radius $1/\lambda_0$ passing through the origin.

4) Using the fact that the object spectrum must be circularly symmetric, rotate step 3) through one revolution to fill in the complete object spectrum.

5) Perform a two-dimensional inverse Fourier transform to recover the object function $k_0^2(\epsilon_r(x,z)-1)$.

Since the resolution distance of the image is $\lambda_0/2$, the computed fields are sampled at 128 points with half wavelength spacing along a line behind the cylinder. Steps 3) and 4) use bilinear interpolation to map the Fast Fourier Transform data to the regular grid on the object spectral matrix.